Star-Shaped Coils in the Transmitter Array for Receiver Rotation Tolerance in Free-Moving Wireless Power Transfer Applications

Pahlavan, Saeideh; Shooshtari, M.; Jafarabadi Ashtiani, Shahin

DOI
10.3390/ en15228643

Publication date
2022

Document Version
Final published version

Published in
Energies

energies

MDPI

Article

Star-Shaped Coils in the Transmitter Array for Receiver Rotation Tolerance in Free-Moving Wireless Power Transfer Applications

Saeideh Pahlavan [1], Mostafa Shooshtari [2,*] and Shahin Jafarabadi Ashtiani [1]

[1] School of Electrical and Computer Engineering, College of Engineering, University of Tehran, Tehran 14395-515, Iran
[2] Laboratory of Electronic Components, Department of Microelectronics, Technology and Materials (ECTM), Delft University of Technology, 2628 CD Delft, The Netherlands
* Correspondence: mostafashooshtari@gmail.com

Abstract: Wireless power is one of the new promising technologies for IoT applications. The use of arrays for power transfer to free-moving objects has revolutionized wireless power transmission (WPT) applications. Herein, we present an extendable platform for transmitting power to a moving object receiving power from an array. The transmitter (TX) consists of two overlapping layers of square planar coils rotated 45 degrees to each other to provide the best electromagnetic flux coverage. Each layer consists of four coils to further control the power supply to the small receiver (RX) coil. This overlapping star-shaped array is stimulated automatically by a power amplifier. This smart stimulation can deliver uniform power to the receiver regardless of rotation and misalignment inconsistencies by using the geometry of the transmitter array. Moreover, by changing the direction of the current of each small square component in each array using the flower-shaped current, a receiver coil perpendicular to the transmitter's plate can obtain power comparable with conventional structures. We use ADS-HFSS simulation to verify the fabrication and measurement results. The proposed transmitter achieves an average of 18.2% power transfer efficiency (PTE) to RX and at 90° angular misalignment, 11.5% PTE, while the conventional structure transfers no power to the perpendicular RX coil. A future application of the transmitter can be the investigation of the neurobehavioral of free-moving animals and brain–machine interface studies in medicine.

Keywords: wireless power transmission; implantable medical device; brain-machine interface; misalignment tolerant

Citation: Pahlavan, S.; Shooshtari, M.; Jafarabadi Ashtiani, S. Star-Shaped Coils in the Transmitter Array for Receiver Rotation Tolerance in Free-Moving Wireless Power Transfer Applications. *Energies* **2022**, *15*, 8643. https://doi.org/10.3390/en15228643

Academic Editors: Yang Li and Pengcheng Zhang

Received: 28 October 2022
Accepted: 15 November 2022
Published: 17 November 2022

1. Introduction

Today, the brain–machine interface (BMI), which has received much attention, is a very useful application for restoring the mobility of disabled patients or moving towards the technology of controlling objects by thinking or moving the eyes such as in neuromorphic [1–3].

In these applications, motor control is obtained by examining recorded brain signals or by stimulating individual brain SUA (single-unit activity) neurons. The BMI can translate neuronal data into commands capable of controlling output software or hardware to carry out the desired action in the same way as a computer or robotic arm [4].

One of the most promising and well-known of these interfaces is optogenetics. Optogenetics is a technique that employs light to control the activity of neurons that have been modified to express light-sensitive ion channels [5]. In this biological technique, the expansion and contraction of muscles or movement are controlled by the optical stimulation of brain or nerve neurons at different points and in different tissues. Optogenetics-based BMI can be used to control urine [6], spine [7] and movement in mice [8].

The stimulation of neurons with blue light with specific wavelength and characteristics was previously controlled by using an optical fiber that was inserted into the scalp of the brain or into the abdominal tissue of mice [9]. These tests are usually long-term, up to one year of testing and review. Therefore, this type of stimulation causes wounds and injuries to the mice. In addition, the free movement of the living object is hampered when using an optical fiber [10].

Stimulation by wireless power transmission (WPT) overcomes these obstacles. WPT stimulation can be used to avoid the utilization of a power supply on the receiver side and enables continuous experiments with live objects [11]. In this type of research, a receiver circuit and coil are implanted inside the body or on the skin tissue of a living animal that consists of a rectifier and a μ-LED for stimulation as a load [12].

Various methods have been provided to power the receiver. Maximum transmission powers, uniform magnetic field and the elimination of blank spots are the reasons for using such methods [13]. Using a coil as large as the dimensions of the cage to cover the moving area of the receiver is one such method [14]. Although the large coil has a simple structure, it needs to be modified due to the nonuniformity of the electromagnetic field as well as the low efficiency [15]. This method was replaced by the idea of the power transmission array because the power transmitted in the center functions as a peak, and the power decreases around the animal behavior test environment or cage. In the coil array method, the movement of the receiver coil is followed by using several transmitters in an array. Power transmission has higher efficiency and is transferred to the receiver in a localized manner [16,17].

Power transmission in arrays has also been expanded by using overlapping array structures to increase power transmission and reduce the dark spots where the vector of the modified field is zero. Using interconnected arrays to automatically position the receiver coil and eliminate multiple peaks in the frequency characteristic of adjacent arrays is one of the most important techniques [18].

In the reported coil array research, a moving object moves on a plane (x-y plane), and movement changes in three dimensions are not considered. Therefore, in the cases where the receiver coil has rotation or misalignment with the transmitter layer, power transmission is interrupted. The use of phase shift in adjacent presentations for cases where the receiver has a 90-degree rotation is one of the methods proposed in the field literature [19]. In these methods, microcontroller, feedback and closed-loop methods are used to estimate the position of the receiver at any moment. Generally, in these methods, artificial intelligence is used to detect the position of the moving object. In this type of array, there is a lookup table based on which the phase shift is applied; in this case, the power is also transmitted to the rotated receiver with the transmitters. Therefore, for each empowerment application, the structure must be redesigned, and the table is updated.

In this paper, two layers of transmitter coils were designed as square and overlapping at 45° angles to each other to shape an 8-folded star shape transmitter coil. This configuration provides increasing transmitted power to the load due to the overlapping of the coils in cases where the receiver has a 90° rotation. In addition, the removal of blank spots is one of the advantages of this structure. By using the proposed transmitters, a uniform electromagnetic field is created at the border between coils without the need for a closed loop and feedback from the microcontroller. This occurs only by arranging the excitation current of each element of the array. Therefore, we have established a semi-uniform field in the moving target area.

First, we will examine the theory and basis of power transmission by presenting and moving the target. Then using the simulator, as well as measuring the field and received power of the built circuits, we show the improved result of the proposed system. As the safety of bio application of WPT is very important, we investigate the biocompability and tissue effect on the proposed system in Section 3.

2. System Basics

The main purpose of this system is the semi-uniform powering of a freely moving living animal survey area. Since the object is moving freely, the power does not reach the receiver in cases where the rotation is more than 0° compared with the transmitter's plate. To solve this problem, two overlapped arrays are used consisting of four-square coils, all of which are simultaneously excited by the power amplifier (PA) . In this case, each of two adjacent square fields of arrays is excited opposite the other. In the border areas of the two transmitter arrays, a weak field is received in the vertical direction due to opposite fields. To investigate the theory, the biovar law is adopted. Figure 1 shows the resultant magnetic field vector at the receiver location between two adjacent transmitter coils. Figure 1A shows two transmitters excited in the same direction; in this case, the receiver has only a vertical resultant magnetic field at the boundary, and the horizontal vector is zero. Therefore, the RX coil receives power when it is oriented horizontally. On the other hand, Figure 1B shows two transmitters excited by currents in opposite directions. In this case, the receiver has a horizontal field at the common boundary, and the vertical field is zero. Therefore, if the receiver rotates 90 degrees, it will receive power.

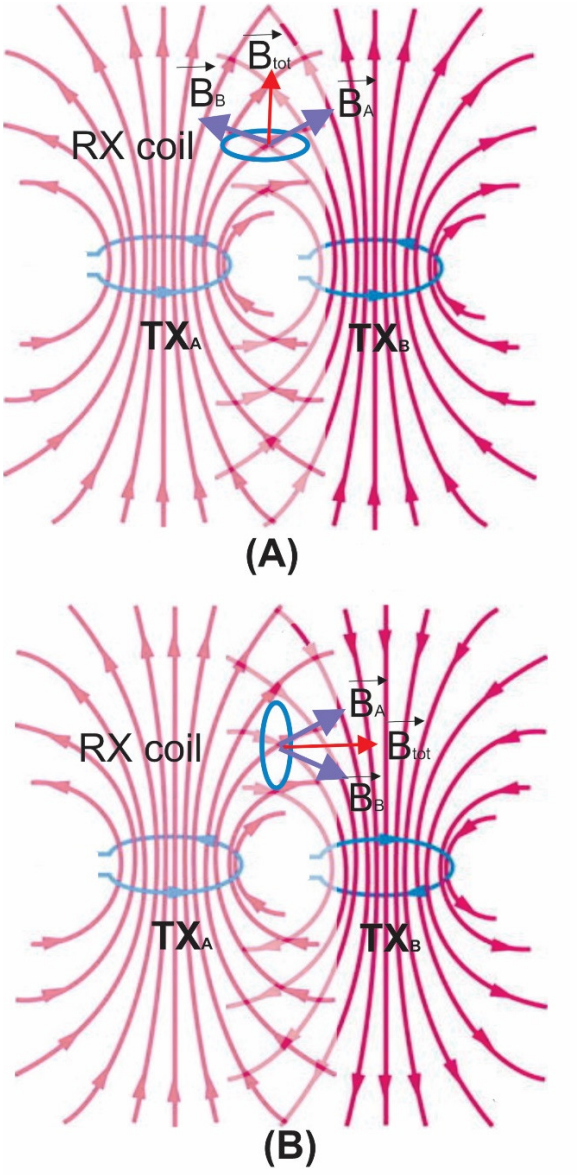

Figure 1. Schematic theory of the resultant vector of the magnetic field at the receiver between two co-excited transmitter coils. Two transmitters are excited in the (**A**) same and (**B**) opposite current

directions. The purple arrows show the EM field vector from each loop. The red arrow shows the total vector.

Next, RX coil orientation scenarios for a free-moving object in the cage area are shown in Figure 2. Number 1 is the horizontal RX module on top of the center TX coils in the array. Number 2 is the horizontal border-located RX module. Numbers 3 and 4 are vertically aligned at the border and on the center-located RX module, respectively. According to each orientation scenario, the power delivery has challenges that interrupt the load current. In the following, by controlling the current excitation direction for each scenario, interrupting the load current is avoided. Adding multiple RX coils in the cage requires that both receivers receive the maximum PTE at the same time. Other issues are also raised such as that each receiver has perfect matching [20]. In this research, we focus on the rotation misalignment, and multiple RX coils need deeper research.

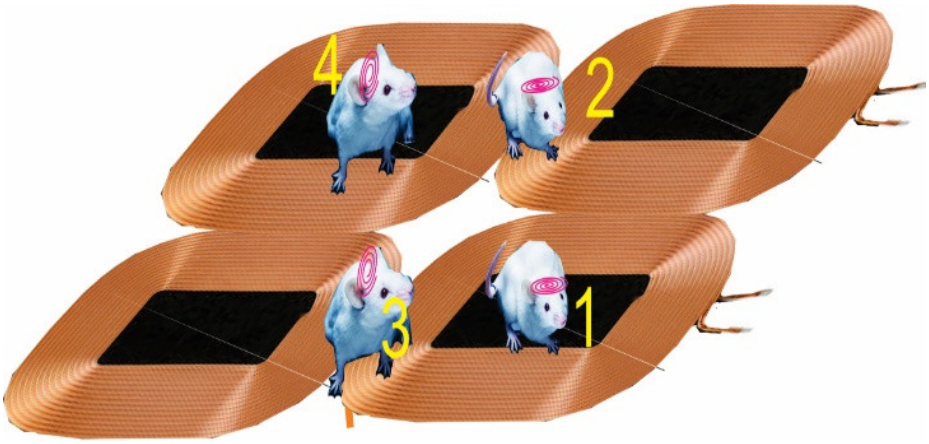

Figure 2. Different mode orientations of the transmitter and receiver coils relative to each other in the wireless power amplifier array. (In positions 1 and 2, the receiver coil is parallel to the transmitter coils, while in positions 3 and 4, the receiver coil makes a 90-degree angle with the transmitter coil).

Figure 3 shows the basics of the proposed transmitter system. Figure 3 shows the excitation directions of two-star shaped arrays; each consists of four TX coil arrays in phase and out of phase based on the right-hand law. Applying the mentioned theory in Figure 1, the use of an array consisting of four transmitter coils arranged for the opposite fields in Figure 3c first causes the field to be received vertically to the horizon receiver at each point in the center of small squares (Figure 2 position 1), and then at the border points (Figure 2 position 2), the horizontal receiver receives no power. Meanwhile, the field at the borders (Figure 2 position 3) for a vertical RX becomes nonzero using an alternative field of Figure 3c.

It can be generalized that if one can divide these small squares into smaller sectors, it is possible to increase the number of areas that we can power to a vertical receiver coil. For example, each small square can be divided into three areas by using three arrays of four oppositely excited coils that make an angle of 30° with each other (see Figure 3a). Therefore, the number of areas that a rotated RX could power triples. These areas could increase proportionally for more plates of arrays. For instance, for a receiver with a size of 4 × 4 cm, using 6 arrays, the whole mouse cage can receive power for the 90° rotation of the receiver.

With the increase in the number of array plates, in addition to the power transmission at the 90° angle of the receiver, the amount of load current received in other places increases due to the overlapping of the transmitters. Of course, at the points where two arrays overlap and the direction of the field is opposite, the field becomes zero. To solve this problem, we used time multiplexing between two arrays.

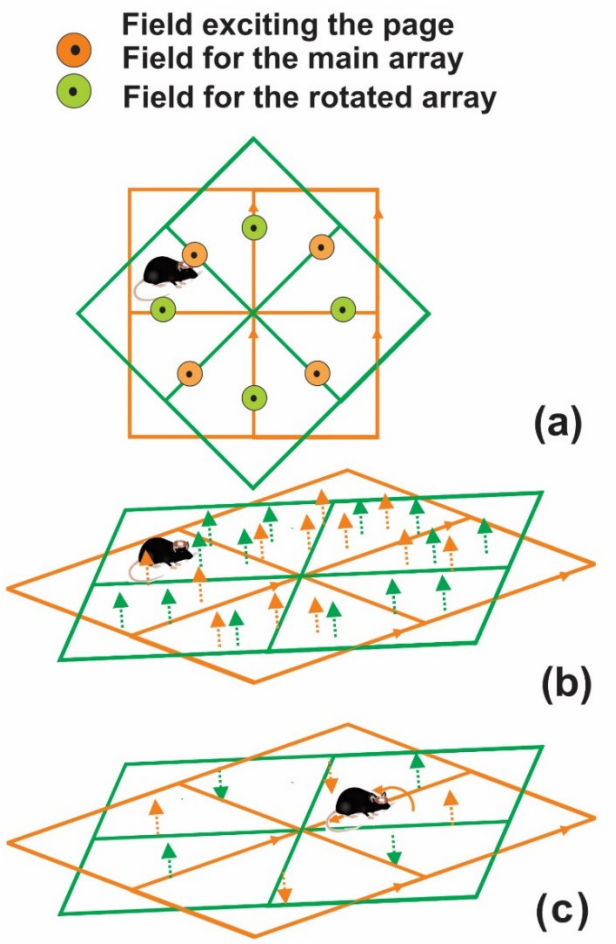

Figure 3. (**a**) Top view and (**b**) side view, in-phase excitation of the arrays. Current flows in opposite directions at the TX border area. (**c**) Out-of-phase excitation in the nearby coils in the vicinity and phase for the second TX array layer. The orange and green arrows show the TX array 1 and 2 EM field vectors respectively.

By using time multiplexing, in addition to saving power consumption, receiver rotation problems are also solved. Therefore, we propose a system with two overlapping arrays in the shape of an eight-pointed star. This system does not need a feedback and receiver position control loop, and by using time multiplexing, only one of these arrays is stimulated by PA at any moment.

Another subject to consider is how to connect each element in each array. These elements are supposed to be stimulated simultaneously but with opposite field vectors. Therefore, we used a parallel connection. The direction of the coils was arranged so that each coil had an opposite field vector from the neighboring coil. The main advantage of using a parallel structure array is providing the same voltage that the PA provides to a single element in the array. In addition, the current of the coil that the receiver is adjacent to is higher, and thus, the magnetic flux is closed between that transmitter and receiver element. Therefore, automatic positioning happens. In this case, power consumption will be optimal. Moreover, when the array is not connected, resonance frequency peaks will happen in several points [18], while using frequency tuning with a capacitor resonance gives only one frequency peak. Other features and relationships that show that parallel structure has advantages were investigated and concluded in our previous research [13].

In order to check the correctness of the aforementioned content, we present a circuit model for the presented system and analyze it mathematically. Figure 4 shows the equivalent circuit model of the proposed TX array. We assumed that when the receiver approached each coil of the transmitter array, for example Coil 1, the only coupling that

could be calculated was the coupling of element K_1 and that the other couplings would be zero ($K_2 = K_3 = K_4 = 0$). The equivalent output voltage for the parallel connected array in case of coupling to coil #1(M_1) is obtained according to Equation (1):

$$\frac{V_{Out}}{V_{in}} = \frac{-R_L j\omega M_s}{\omega^2 M_1^2 + Z_{Ls} Z_L} \quad (1)$$

where R_L and Z_L are the load side impedance. L_{11}, C_1 and R_1 show the primary side parasitic elements. Z_s is input impedance of the primary side. At each position of the receiver module, the nearest coil in the array makes Ki with the RX coil. Therefore, the positioning of the mice in the array is smart and automatic. The other TX coil currents are approximately zero.

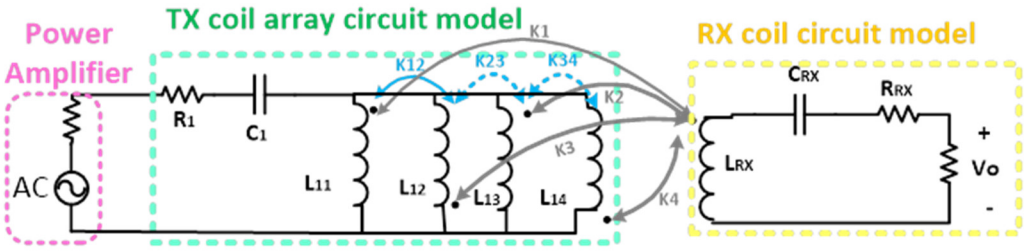

Figure 4. Circuit equivalent model of WPT array. The pink, green and yellow box shows the PA, TX coil tunning and RX coil tunning circuits respectively.

3. Simulation and Measurement Results

The performance of the overlapped eight-star shaped array driven by a sinusoidal carrier signal was investigated by simulation and experimental methods. A high-frequency structure simulator (HFSS, ANSYS, Canonsburg, PA, USA) and an advanced simulator design system (ADS, Agilent, Santa Clara, CA, USA) were applied as proof of concept.

The simulation in HFSS using copper for the coils and FR-4 substrate were placed, and the surrounding environment was air. The performance frequency was analyzed at 10 MHz, and the tuning capacitance for dominant resonance frequency was added as a boundary to the simulator. The solution type is modal network analysis.

The block diagram in Figure 5 was used to test and apply excitation by PA to the transmitter arrays in this paper. There are two plates, each consisting of four TX coils for freely moving mice and optogenetics behavioral experiments. The RX coil and circuit with two blue μ-LEDs are located on the heads of the mice. As can be seen from Figure 5, the transmitter coils are excited by PAs.

A class D PA drove two arrays of parallel connected TX coil. This PA switched between two arrays in a time-interleaved of 100 msec with a STM32 microcontroller (Figure 5). There was no need for a sophisticated closed loop for determining the RX coil position or MCU. The whole system operates smartly, and the current is drawn from the TX element coil in each array that is closest to the RX coil [16].

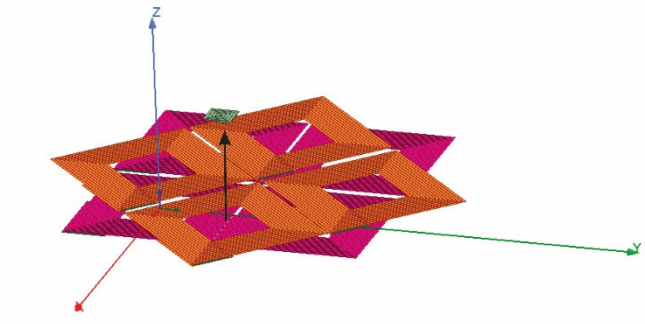

(**a**)

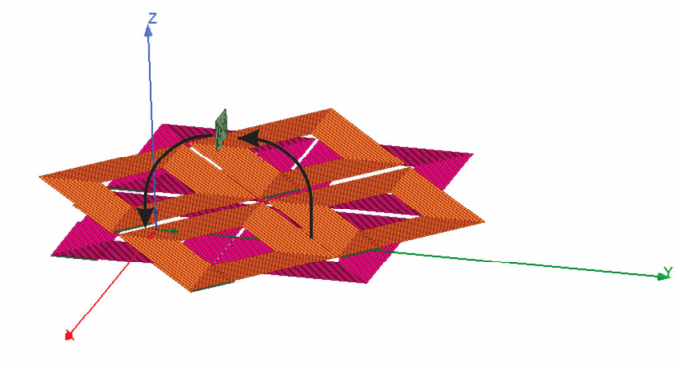

(**b**)

Figure 5. Electromagnetic field simulation using HFSS. The field distribution for (**a**) horizontal and (**b**) vertical RX module.

The field flux is closed between the receiver and the coil of the array that is closest to the receiver.

On the other hand, since both arrays are turned on at a time interval of 100 milliseconds, the receiver receives the same amount of power from both sides.

Figure 5 shows the simulation results of the field flux. In the case that the receiver is in the 90° position and at the border between both transmitters, it receives power due to the opposite current of each neighboring coil.

To verify the theory obtained in part II, several measurements were taken, and coils were fabricated to prove the results of simulations and theories with experimental measurements. The test schematics are presented in Figure 6.

Many factors affect simulation and measurement results such as simulator accuracy for coverage, parasitic elements, connections and SMA ports [21].

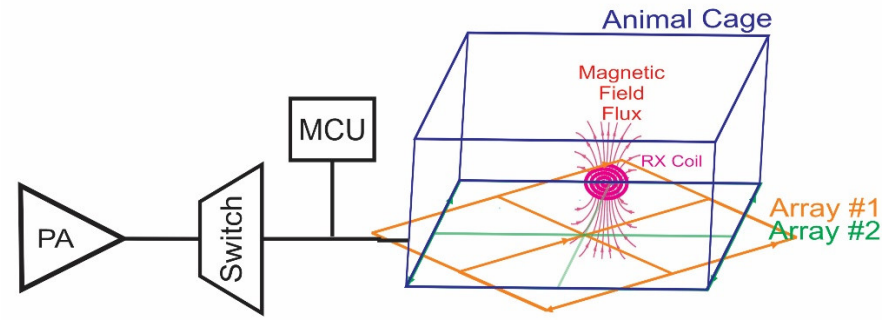

Figure 6. Schematic of measurement setup for proposed array configuration. The orange and green array are the first and second TX array swOitch respectively.

A block diagram and measurement setup of the WPT system including transmitter coils and receiver circuits designed for the moving object are presented in Figure 7. According to Figure 7a, array inductances are excited by a class D amplifier using a tuning capacitance to work on 10 MHz resonance frequency. The N-channel IRF640 MOSFET and non-inverse IR2110 MOSFET driver between the signal generator and MOSFET were used to set up the PA. More details about the experimental setup are addressed in [13,19].

The fabricated and measurement setup for the RX module is presented in Figure 7b,c. To prevent unwanted battery discharge by reverse current, the load battery is connected in series with Schottky diodes. The battery transmits the generated wireless DC power to the load and the μ-ILED for wireless operation. The performance of the proposed sample with important parameters such as transfer coefficient PTE and PDL was measured and reported [22,23].

According to [13], improving the coil's quality efficiency and amplifying the coupling factor cause link efficiency improvement. The inner (ID) and outer (OD) diameters, which are two of the most fundamental geometry parameters of coils, were examined. Six different coils with different ID and turns were fabricated, and their parameters were measured. According to WPT coil design relations, the size of coils has an impact on parasitic resistance Rs, and Rs reduces coil quality (Q). There is a tradeoff between ID, number of turns (n), spacing between turns (S) and layer number of wires in the coil to achieve maximum quality factor and PTE. The parasitic parameters such as L, R and C of each coil plus quality factors are theoretically calculated based on equations in [13]. Moreover, the measured parasitic are performed using GW Instek LCR-8210 LRC Meter.

In this article, we used square coils to have a symmetrical and geometrical structure. To improve the efficiency of the inductive link in this structure, there are many methods such as using ferrite to increase the efficiency, reduce the power transmission distance and increase the number of turns of the coils [24]. The proposed structure has better efficiency compared with the circular coil structure in the array. In addition to the increase in transmission distance, which causes a major reduction in PTE, if smaller coils are used, a greater drop in efficiency is observed [24]. Using the relationship mentioned in the literature, the optimal array for induction link can be designed. More turns create larger inductance while lowering the quality. For overall PTE, there are some tradeoffs between coil design parameters [13,21].

The measured current and voltage delivered to the load shows the power delivery to the load (PDL). The WPT system is fabricated and simulated with copper PCB coils, as shown in Figure 7b,c. The transmitter part of magnetic resonance WPT includes two arrays, each containing 4 coils, which consists of eight turn spiral resonator. Each TX resonators in this work have a square shape with a width of 18.8 cm, a strip width of 2.5 mm, and an inter-strip space of 1 mm. This structure is fabricated on a 0.5 mm FR-4 substrate with a thickness of 0.35 μm copper and has a dielectric constant of 4.4. The resonant frequency of the resonator can be controlled by an external capacitor embedded in the gap of two spiral ends. The receiver part has the same structure with a 4 cm square PCB coil and a 40 mm distance from TX array coils Figure7. The fabricated coil's specifications are listed in Table 1.

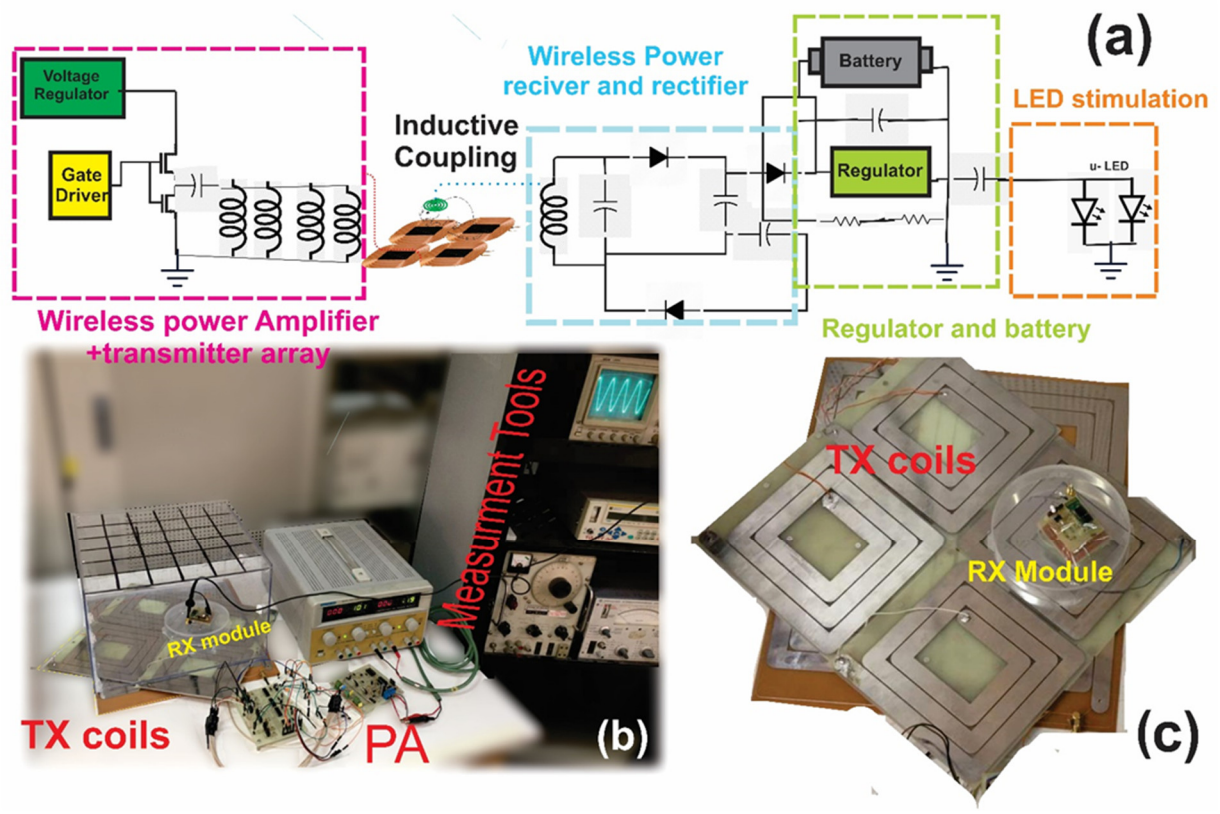

Figure 7. Schematic and Measurement setup of proposed WPT configuration. (**a**) Schematic block diagram of the measurement setup. (**b**) Measurement set up and test setup using array and the RX module and measurement equipment and (**c**) fabricated star shaped coils and RX module.

Table 1. Specification of the fabricated coils.

	Receiver Coil	Transmitter Coil
Size (mm)	40 × 40	160 × 160
Number of turns (N)	4	3
Spacing (mm)	0.5	1
Inductance (μH)	1	0.9
Quality Factor	77	182

The receiver consists of PCB coil antenna and Li-ion battery and RX circuit for running the μ-iLED in optogenetics applications, Figure 8. The receiver circuit is consisting of full wave rectifier with Schottky diodes, regulator and μ-iLED as loads Figure 7a.

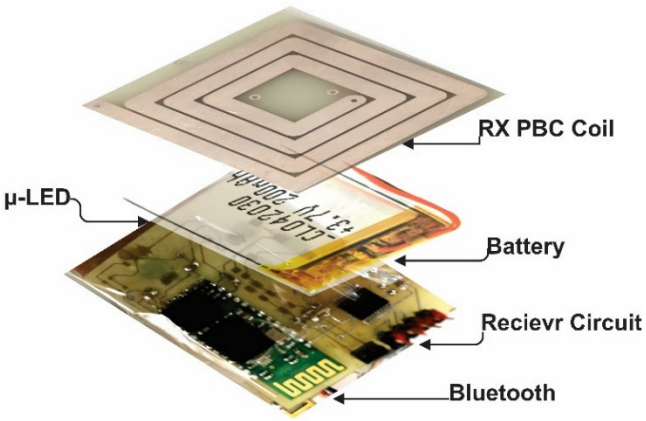

Figure 8. Receiver Module layers consist of RX PCB antenna, Li-ion Battery and rectifier and Bluetooth circuit.

The cage is covered with two 32 × 32 cm sized TX arrays. The voltage waveform was measured by a digital oscilloscope (GW Instek GDS-3000), Figure 9.

Figure 9 shows the measured output voltage of the PA and the load-delivered voltage in the presence of an 82 Ω load. The RMS input current of the circuit was measured to be about 80 mA. The input of the PA is a pulse with amplitude of about 10 V peak to peak. The output current was recorded at 73 mA. The delivered power to the load is measured 146 mW. Moreover, for 90° rotated RX coil the output voltage of the TX coil (blue line) and regulated load output voltage (yellow line) are measured in Figure 9b. According to the measurements, the output current of 50.54 mA are recorded for a 90°-oriented RX coil with 92 mW power delivery to the load, which gives system efficiency of 11.5%.

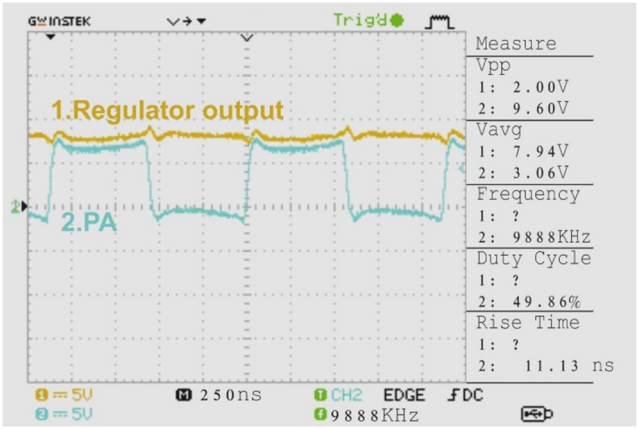

(**a**)

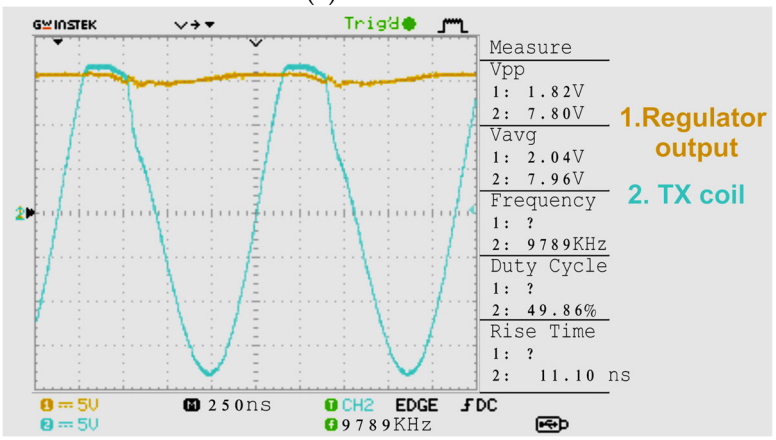

(**b**)

Figure 9. Measurement results. (**a**) Measured regulator voltage and PA waveform by a digital oscilloscope. Yellow line shows the rectifier output voltage and blue line shows the PA output voltage at 0° rotation orientation. (**b**) TX coil voltage blue line and regulator output voltage for 90° rotated RX coil in yellow line.

Figure 10 shows the measured and simulation results of the received power on the receiver side at different locations of the receiver on top of the transmitter array. We got the data from measurements at borders and middle point of each triangle created between plates in Figure 3 and used MATLAB to visualize the measurement data in Figure 10. Figure 9a,b shows the delivered power to the load at 4 cm distance with one-layer TX array and star shaped TX array. For simulation results Figure 10c,d, the s-parameter result obtained from HFSS are entered the ADS block diagram to obtain the Magnetic field and distribution. The difference between the field and PDL distribution in the case of the simple array and the Star-shaped array is evident in Figure 10. The proposed array has a more uniform coverage area than the conventional presentation. It also has the advantage of covering the rotation area of the receiver, which is not seen in the common type.

3D distribution of the magnetic field in Figure 10 shows how to aggregate the power transmission area in overlapping mode and star array. As it can be seen from the figure, the coverage area of the power transmission has been doubled compared to the conventional mode. Also, at the borders of each plate which is 8 zones the rotating RX coil receives power while in the conventional arrays it doesn't. according to the Figure 10, the difference between the measurement and simulated PDL are due to the SMA connectors effect and parasitic effect of cable and circuit elements and also parasitic mismatch between coils in the array.

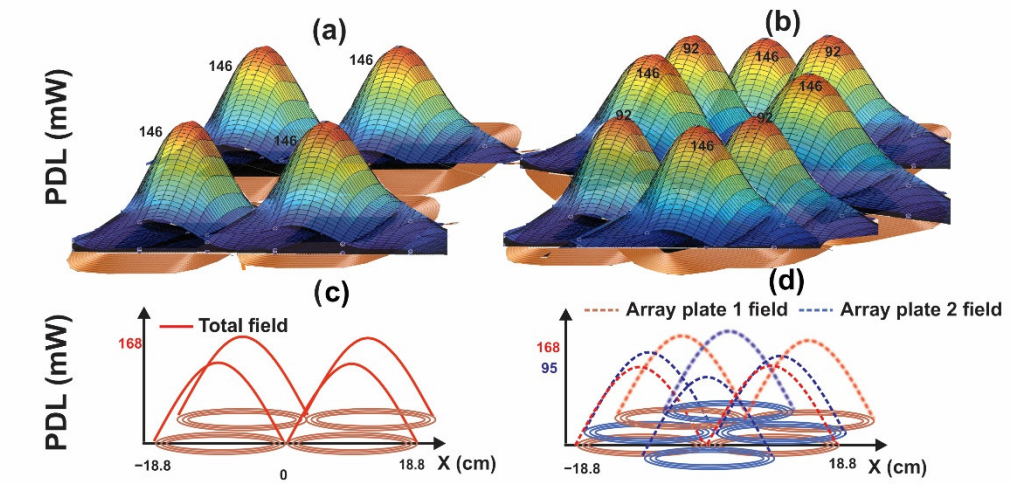

Figure 10. Power distribution and PDL for horizontal (*x*-*y*) RX Movement between the arrays. (**a**) Conventional array and (**b**) 8-folded star shape array measured PDL peak. (**c**) Conventional arrays and (**d**) 8-folded star shape array PDL peak distribution.

The animal's tissue will have an important effect on the received power. This effect will be in the form of a reduction in the power received in the animal's head coil. Tissue is lossy and variable, and safety is a concern due to the absorption of electromagnetic energy in high-water-content tissue. Although the effect of reducing the received power is much greater for an implant inside the body, coil implants adjacent to the body tissue will not be unaffected by this reduction [25].

The effect of living animal tissue, which includes body tissue, skin, blood and water, in the HFSS simulation software, under the title of SAR (specific absorption rate) simulation, showed the maximum absorption rate of electromagnetic radiation in living animal tissue, to not exceed the standard amount.

SAR was simulated to check the biocompatibility of living tissue with the proposed array. The SAR simulation in ANSYS HFSS™ at 10 MHz (ISM band) is shown in Figure 11 for 10 W input powers. The SAR obtained at this operating frequency at a distance of 4 cm is 0.20 mW/kg, lower than the IEEE standard of 2 W/kg for 10 g of tissue [12,25].

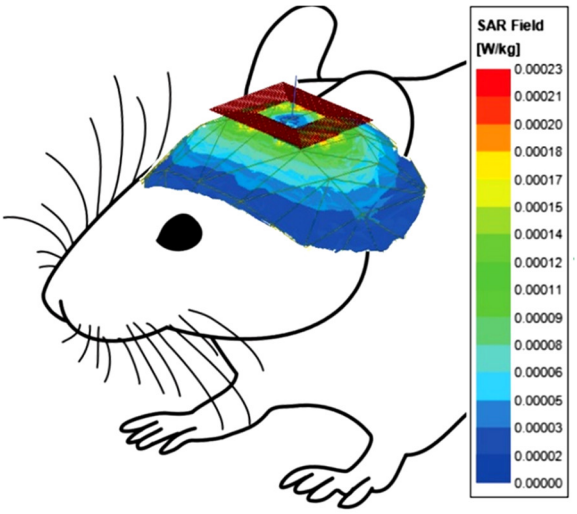

Figure 11. 3D SAR simulation for a living tissue for bio-medical compatibility.

4. Conclusions

In this paper, a new arrangement of power transmission arrays to moving objects is presented for animal behavior research applications. This array solves the problems of receiver rotation and power transmission interruption.

These methods are different from the previously presented methods that used large coils. Large coils brought lower gain and power loss in the side areas.

Using the magnetic field theory and Biosavar's law, as well as arrays connected in parallel, the idea of the work was investigated. Additionally, using field simulation and making and measuring test circuits, the power received by the eight-cornered star array was tested. The test results showed that the presented array increases the received power up to 146 mW, while in the case of the rotation of the receiver, the power transmission also improved by 92 mW. Compared with the conventional structures, practically no power was received by rotation.

Author Contributions: Conceptualization, S.P.; methodology, S.P.; software, S.P.; validation, S.P. and M.S.; formal analysis, S.P.; investigation, S.P.; resources, S.P. and M.S.; data curation, S.P.; writing—original draft preparation, S.P. and M.S.; writing—review and editing, S.P. and M.S.; visualization, S.P. and M.S.; supervision, S.J.A.; project administration, S.P. and M.S. All authors have read and agreed to the published version of the manuscript.

Funding: This research received no external funding.

Data Availability Statement: The data presented in this study are available from the corresponding authors upon reasonable request.

Conflicts of Interest: The authors declare no conflicts of interest.

References

1. Musk, E. An integrated brain-machine interface platform with thousands of channels. *J. Med. Internet Res.* **2019**, *21*, e16194.
2. Wu, N.; Wan, S.; Su, S.; Huang, H.; Dou, G.; Sun, L. Electrode materials for brain–machine interface: A review. *InfoMat* **2021**, *3*, 1174–1194.
3. Sharma, R.; Kim, M.; Gupta, A. Motor imagery classification in brain-machine interface with machine learning algorithms: Classical approach to multi-layer perceptron model. *Biomed. Signal Process. Control* **2022**, *71*, 103101.
4. Andersen, R.A.; Aflalo, T.; Bashford, L.; Bjånes, D.; Kellis, S. Exploring Cognition with Brain–Machine Interfaces. *Annu. Rev. Psychol.* **2022**, *73*, 131–158.
5. Hramov, A.E.; Maksimenko, V.A.; Pisarchik, A.N. Physical principles of brain–computer interfaces and their applications for rehabilitation, robotics and control of human brain states. *Phys. Rep.* **2021**, *918*, 1–133.
6. Zhou, Z.; Liao, L. Optogenetic Neuromodulation of the Urinary Bladder. *Neuromodulation Technol. Neural Interface* **2021**, *24*, 1229–1236.

7. Zhang, Q.; Hu, S.; Talay, R.; Xiao, Z.; Rosenberg, D.; Liu, Y.; Sun, G.; Li, A.; Caravan, B.; Singh, A.; et al. A prototype closed-loop brain–machine interface for the study and treatment of pain. *Nat. Biomed. Eng.* **2021**, 1–13. https://doi.org/10.1038/s41551-021-00736-7.
8. Lee, J.H.; Lee, S.; Kim, D.; Lee, K.J. Implantable Micro-Light-Emitting Diode (μLED)-based optogenetic interfaces toward human applications. *Adv. Drug Deliv. Rev.* **2022**, *187*, 114399.
9. Tsunematsu, T.; Tanaka, K.; Yamanaka, A.; Koizumi, A. Ectopic expression of melanopsin in orexin/hypocretin neurons enables control of wakefulness of mice in vivo by blue light. *Neurosci. Res.* **2013**, *75*, 23–28.
10. Nurmikko, A.V.; Donoghue, J.P.; Hochberg, L.R.; Patterson, W.R.; Song, Y.-K.; Bull, C.W.; Borton, D.A.; Laiwalla, F.; Park, S.; Ming, Y.; et al. Listening to Brain Microcircuits for Interfacing with External World—Progress in Wireless Implantable Microelectronic Neuroengineering Devices. *Proc. IEEE* **2010**, *98*, 375–388.
11. Biswas, D.K.; Sinclair, M.; Hyde, J.; Mahbub, I. An NFC (near-field communication) based wireless power transfer system design with miniaturized receiver coil for optogenetic implants. In Proceedings of the 2018 Texas Symposium on Wireless and Microwave Circuits and Systems (WMCS), Waco, TX, USA, 5–6 April 2018; IEEE: Piscataway, NJ, USA, 2018; pp. 1–5.
12. Zhou, Y.; Liu, C.; Huang, Y. Wireless Power Transfer for Implanted Medical Application: A Review. *Energies* **2020**, *13*, 2837.
13. Pahlavan, S.; Shooshtari, M.; Maleki, M.; Ashtiani, S.J. Using Overlapped Resonators in Wireless Power Transfer for Uniform Electromagnetic Field and Removing Blank Spots in Free Moving Applications. *Electronics* **2022**, *11*, 1204.
14. Jow, U.-M.; McMenamin, P.; Kiani, M.; Manns, J.R.; Ghovanloo, M. EnerCage: A Smart Experimental Arena with Scalable Architecture for Behavioral Experiments. *IEEE Trans. Biomed. Eng.* **2013**, *61*, 139–148.
15. Jia, Y.; Wang, Z.; Mirbozorgi, S.A.; Ghovanloo, M. A closed-loop wireless homecage for optogenetic stimulation experiments. In Proceedings of the 2015 IEEE Biomedical Circuits and Systems Conference (BioCAS), Atlanta, GA, USA, 22–24 October 2015.
16. Mirbozorgi, S.A.; Bahrami, H.; Sawan, M.; Gosselin, B. A Smart Multicoil Inductively Coupled Array for Wireless Power Transmission. *IEEE Trans. Ind. Electron.* **2014**, *61*, 6061–6070.
17. Bahrami, H.; Mirbozorgi, S.A.; Nguyen, A.T.; Gosselin, B.; Rusch, L.A. System-Level Design of a Full-Duplex Wireless Transceiver for Brain–Machine Interfaces. *IEEE Trans. Microw. Theory Tech.* **2016**, *64*, 3332–3341.
18. Mirbozorgi, S.A.; Maghsoudloo, E.; Bahrami, H.; Sawan, M.; Gosselin, B. Multi-resonator arrays for smart wireless power distribution: Comparison with experimental assessment. *IET Power Electron.* **2020**, *13*, 4183–4193.
19. Waters, B.H.; Mahoney, B.J.; Ranganathan, V.; Smith, J.R. Power Delivery and Leakage Field Control Using an Adaptive Phased Array Wireless Power System. *IEEE Trans. Power Electron.* **2015**, *30*, 6298–6309.
20. Cai, W.; Ma, D.; Tang, H.; Lai, X.; Liu, X.; Sun, L. Highly Efficient Target Power Control for Two-Receiver Wireless Power Transfer Systems. *Energies* **2018**, *11*, 2726.
21. Van Schuylenbergh, K.; Robert, P. (Eds.) *Inductive Powering: Basic Theory and Application to Biomedical Systems*; Springer: Dordrecht, The Netherlands, 2009.
22. El Rayes, M.M.; Nagib, G.; Abdelaal, W.A. A review on wireless power transfer. *Int. J. Eng. Trends Technol. IJETT* **2016**, *40*, 272–280.
23. Zhang, Z.; Pang, H.; Georgiadis, A.; Cecati, C. Wireless power transfer—An overview. *IEEE Trans. Ind. Electron.* **2018**, *66*, 1044–1058.
24. Stankiewicz, J.M.; Choroszucho, A. Efficiency of the Wireless Power Transfer System with Planar Coils in the Periodic and Aperiodic Systems. *Energies* **2022**, *15*, 115.
25. Bocan, K.N.; Mickle, M.H.; Sejdić, E. Multi-disciplinary challenges in tissue modeling for wireless electromagnetic powering: A review. *IEEE Sens. J.* **2017**, *17*, 6498–6509.